



Continuous Hyperplastic Models for Overconsolidated Clays

I. EINAV

Centre for Offshore Foundation Systems
University of Western Australia
Crawley, Perth WA 6009
eina@cylle.uwa.edu.au

A. M. PUZRIN

School of Civil and Environmental Engineering
Georgia Institute of Technology
790 Atlantic Drive, Atlanta, GA 30332-0355, U.S.A.

G. T. HOULSBY

Department of Engineering Science, Oxford University
Oxford, OX1 3PJ, U.K.
guy.houlsby@eng.ox.ac.uk

Abstract—This paper presents four constitutive models for prediction of the behaviour of overconsolidated clays under triaxial loading conditions. Their formulations are based on a new continuous hyperplastic framework. Continuous hyperplasticity allows the derivation of plasticity models which simulate smooth stress-strain behaviour, have continuous memory, and are guaranteed to obey the laws of thermodynamics. All four models are capable of simulating the triaxial stress-strain behaviour of overconsolidated clays in a wide strain range. The ability of the models to predict the stress path dependency of the clay behaviour is evaluated against experimental data obtained on undisturbed Laval samples of Bothkennar clay. © 2003 Elsevier Science Ltd. All rights reserved.

Keywords—Clays, Constitutive relations, Continuous hyperplasticity, Laboratory tests, Stiffness.

1. INTRODUCTION

Continuous hyperplasticity is a novel approach to plasticity, and is utilized in this paper as a framework for construction of new constitutive models. Puzrin and Houlsby [1,2] develop in detail the continuous hyperplastic approach as a generalization of hyperplasticity. Hyperplasticity is based on the work of Ziegler [3] and is described in [4–6]. The advantage of hyperplasticity is that it allows for the derivation of plasticity models which are guaranteed to obey the laws of thermodynamics. The hyperplastic formulation is based on extensive use of internal variables (normally associated with plastic strains) and allows for the specification of any constitutive model solely by two scalar potential functions: an energy function and a dissipation function. Unfortunately, hyperplasticity is unable to describe the case of continuous field of yield surfaces (e.g., [7]), and therefore models developed within this framework exhibit an abrupt change from

This research was supported by the Fund for the Promotion of Research at the Technion.

elastic to elastic-plastic behaviour. The advantage of continuous hyperplasticity is that it allows the models to simulate continuous memory and smooth transitions in stress-strain behaviour. The generalization of hyperplasticity to continuous hyperplasticity is based on utilization of internal functions instead of variables, so that the constitutive models are formulated in terms of two scalar potential *functionals* (rather than functions as in hyperplasticity).

In [8] the continuous hyperplasticity approach has been used to define a model for triaxial behaviour of overconsolidated clays within a small strain region of high stiffness. The purpose of this paper is to introduce and evaluate new continuous hyperplastic constitutive models in an attempt to describe material behaviour in a wide strain range in a unified manner. The derivation of incremental response from the two potential functionals is discussed elsewhere [1]. In this paper, we limit the description of the proposed models to presentation of their potential functionals which are entirely sufficient to specify each model. Being formulated as continuous hyperplastic, these models are automatically guaranteed not to violate thermodynamic principles.

The four proposed models can be divided into two conceptual types: Puzrin and Burland [8] model type (PB), and a continuous hyperplastic modified cam clay field of yield surface model type (CHMCC). The PB type models extend an existing small strain model [9] to simulate soil behaviour beyond the small-strain region, with an emphasis still on accurate prediction of the small strain stiffness. The CHMCC type models are focused on accurate simulation of soil behaviour beyond the small-strain region. The models are evaluated against experimental data obtained on undisturbed Laval samples of Bothkennar clay by Smith [10].

2. AUTOMATIC DERIVATION OF INCREMENTAL RESPONSE

Normally, a new constitutive model would require a new procedure for derivation of the incremental response. However, for the models generated within the framework of continuous hyperplasticity [1], this derivation has been unified and is performed automatically by a computer program written in the 'Mathematica 4' computing environment.

The program requires two potential functionals to define a model. A complete derivation of incremental relations for the constitutive model is then automatically produced and the entire constitutive response for specified loading conditions (stress, strain, or mixed control) can be obtained. The process of constitutive modelling becomes almost automatic. An advantage of the new continuous hyperplastic approach is in the compactness of its formulation: two scalar potential functionals define a model completely. By modifying these functionals, new models can be easily derived to improve the prediction of the stress-strain behaviour of soils.

3. PUZRIN AND BURLAND (PB) TYPE MODELS

The PB models put a particular emphasis on the accurate simulation of soil behaviour within the small strain region of high stiffness. The clay behaviour within this strain range is extensively described in [11–14]. Puzrin and Burland [14] presented a plasticity model for the small strain triaxial behaviour of overconsolidated clays. The model employed an inner yield surface (Y1), which encloses a region of stress space in which the response is purely elastic, and an outer surface (Y2) representing the outer boundary of highly nonlinear behaviour. Once the outer surface is reached, further monotonic loading along any straight effective stress path does not cause changes in soil stiffness. If the stress point lies between these two surfaces, the plastic strains are calculated using an empirically determined logarithmic relationship.

Puzrin, Houlsby and Burland [9] reformulated this model within the continuous hyperplastic method. The model lacks any features which relate to gross plastic strains or to failure; nonetheless, it was the first time continuous hyperplasticity had been used to define a nontrivial model for soil behaviour. Puzrin and Burland [8] approached the gross plastic strain problem by adding a third elliptical yield surface (Y3, which is actually the modified cam clay large-scale yield surface)

to the original model [14]. However, it was formulated using the concepts of conventional kinematic hardening plasticity and could not claim the advantages of the continuous hyperplasticity. In this paper, the PB models are developed by adding a Y3 surface to the model [9], but within the continuous hyperplastic framework.

3.1. Puzrin and Burland Model 1 (PB1)

The model requires nine parameters, which can be determined from a single consolidated undrained triaxial test with local deformation measurements [8]. Five of the parameters are required for the description of the modified cam clay (MCC) yield surface, and the rest are for the description of soil behaviour within the small strain region; all the parameters are independent and have physical meaning. The complete derivation of the PB1 model is not presented here. However, a similar model, though without the outermost yield surface, was described in [9].

The first functional required for the model definition can be either the specific Helmholtz free energy or the specific Gibbs free energy. For the sake of brevity, let us introduce only the Gibbs free energy functional

$$g[\sigma, \hat{\alpha}, \alpha^{**}] = -\frac{1}{2}(\sigma - \sigma_0)^\top D^{-1}(\sigma - \sigma_0) - (\sigma - \sigma_0) \int_0^1 \hat{\alpha}(\eta) d\eta - \sigma \alpha^{**} + \frac{1}{2} \int_0^1 h(\eta) \hat{\alpha}(\eta)^\top B^{-1} \hat{\alpha}(\eta) d\eta. \quad (1)$$

The second functional is the dissipation functional

$$d^g[\dot{\alpha}, \hat{\alpha}, \dot{\alpha}^{**}, \alpha^{**}] = \int_0^1 a(\eta) x[\hat{\alpha}_v, \alpha_v^{**}] \sqrt{\dot{\hat{\alpha}}(\eta)^\top B^{-1} \dot{\hat{\alpha}}(\eta)} d\eta + p_{x0} x[\hat{\alpha}_v, \alpha_v^{**}] \left(\sqrt{(\dot{\alpha}_v^{**})^2 + M^2 (\dot{\alpha}_s^{**})^2} + \dot{\alpha}_v^{**} \right), \quad (2)$$

where

$$x[\hat{\alpha}_v, \alpha_v^{**}] = \exp \frac{\int_0^1 \hat{\alpha}_v(\eta) d\eta + \alpha_v^{**}}{\lambda - \kappa}.$$

The effective stresses in triaxial stress space are defined by the vector $\sigma = \{p', q\}^\top$; the initial stresses are defined by the vector $\sigma_0 = \{p'_0, q_0\}^\top$. The internal variable function for the behaviour between the linear elastic region (Y1) and the small strain region (Y2) is defined by the vector $\hat{\alpha} = \{\hat{\alpha}_v, \hat{\alpha}_s\}^\top$, while the internal variable vector related to the large-scale yield surface (Y3) is given by $\alpha^{**} = \{\alpha_v^{**}, \alpha_s^{**}\}^\top$. Parameters λ and κ represent the slopes of the virgin compression line and the elastic swelling line in $\ln v - \ln p'$ space, as discussed in [15]. The parameter p_{x0} is the initial coordinate of the centre of the Y3 yield surface. The elastic stiffness matrix is defined by $D = \begin{bmatrix} K & 0 \\ 0 & 3G \end{bmatrix}$, where K and G are the bulk and the shear modulus. The matrix B is defined by

$$B = \frac{|D|}{3G} D^{-1} = \begin{bmatrix} 1 & 0 \\ 0 & n^2 \end{bmatrix},$$

where $n^2 = K/3G$. The semidiameter of each elliptical yield surface between Y_1 and Y_2 in the p -direction is defined by the function $a(\eta) = a_e + \eta(a_L - a_e)$. The parameter a_e defines the size of the inner yield surface (within which behaviour is purely elastic), and a_L is the size of the Y_2 surface (defining the outer limit of the variable stiffness region). The function $h(\eta)$ was defined in [9], and defines the shape of the normalized logarithmic curve. The dissipation functional

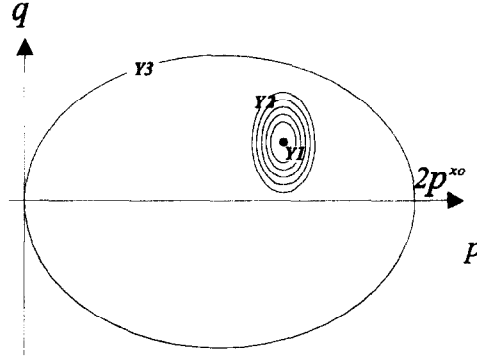


Figure 1. Initial orientation of the PB1 and PB2 yield surfaces.

produces a field of elliptical yield functions between Y1 and Y2 which are centered around the initial stress state, plus an MCC surface Y3 (see Figure 1).

3.2. Puzrin and Burland Model 2 (PB2)

This model is a modification of the PB1 model, which allows a more accurate simulation of soil behaviour at intermediate strains. The model requires only one additional curve fitting parameter (h^*) in addition to the above PB1 model, which allows control of the slope of the stress-strain curve between the small strain region of high stiffness (Y2) and the large-scale yielding region (Y3). The internal variable vector $\alpha^* = \{\alpha_v^*, \alpha_s^*\}$ is an additional plastic strain vector that relates to the translation of Y2 surface. In this case, the Gibbs free energy functional is expressed in the form

$$g[\sigma, \hat{\alpha}, \alpha^*, \alpha^{**}] = -\frac{1}{2}(\sigma - \sigma_0)^T D^{-1}(\sigma - \sigma_0) - (\sigma - \sigma_0) \int_0^1 \hat{\alpha}(\eta) d\eta - (\sigma - \sigma_0)\alpha^* - \sigma\alpha^{**} \\ + \frac{1}{2} \int_0^1 h(\eta) \hat{\alpha}(\eta)^T B^{-1} \hat{\alpha}(\eta) d\eta + \frac{1}{2} h^* \alpha^{*T} B^{-1} \alpha^*, \quad (3)$$

and the dissipation functional is written as

$$d^G [\dot{\hat{\alpha}}, \hat{\alpha}, \dot{\alpha}^*, \dot{\alpha}^{**}, \alpha^*, \alpha^{**}] = \int_0^1 a(\eta) x [\dot{\alpha}_v, \alpha_v^*, \alpha_v^{**}] \sqrt{\dot{\hat{\alpha}}(\eta)^T B^{-1} \dot{\hat{\alpha}}(\eta)} d\eta + x [\dot{\alpha}_v, \alpha_v^*, \alpha_v^{**}] \\ \times \left(a_L \sqrt{\dot{\alpha}^{*T} B^{-1} \dot{\alpha}^*} + p_{x0} \left(\sqrt{(\dot{\alpha}_v^{**})^2 + M^2 (\dot{\alpha}_s^{**})^2} + \dot{\alpha}_s^{**} \right) \right), \quad (4)$$

where

$$x[\dot{\alpha}_v, \alpha_v^*, \alpha_v^{**}] = \exp \frac{\int_0^1 \dot{\alpha}_v(\eta) d\eta + \alpha_v^* + \alpha_v^{**}}{\lambda - \kappa}.$$

The dissipation functional produces a field of elliptical yield functions between Y1 and Y2, an additional yield function exactly on the Y2 border, plus a modified cam clay surface Y3. The orientation of the yield surfaces stays exactly as the PB1 model (see Figure 1).

4. CONTINUOUS HYPERPLASTIC MODIFIED CAM CLAY (CHMCC) TYPE MODELS

While the PB models are focused on the simulation of small strain region of high stiffness, the purpose of the CHMCC models is an accurate simulation of stress-strain behaviour beyond this region and up to failure. This task allows a significant reduction in the number of parameters and simplification of the equations of potential functionals defining the models. The dissipation functionals of the CHMCC models result in a field of mixed hardening modified cam clay (MCC) yield surfaces. In addition, the CHMCC model utilizes a hyperbolic type of stress-strain relation in order to characterize the stiffness variation during loading.

4.1. Continuous Hyperplastic MCC Model (CHMCC1)

The model requires six parameters: five parameters for the MCC yield surfaces which can be determined as in the classical parameter derivation for the modified cam clay; one additional parameter determines the shape of the stress-strain curve inside the large-scale yield surface. The model is defined by the following two scalar potential functionals. The Gibbs free energy is written as

$$g[p, q, \hat{\alpha}] = -\kappa p \left(\log \left(\frac{p}{p_0} \right) - 1 \right) - \frac{q^2}{6pG} - \left(p \int_0^1 \hat{\alpha}_v d\eta + q \int_0^1 \hat{\alpha}_s d\eta \right) + \int_0^1 \frac{(1-\eta)^3}{2(c-1)} \frac{(p/\kappa)\hat{\alpha}_v^2 + 3pG\hat{\alpha}_s^2}{2} d\eta + (\lambda - \kappa)p_{x0} \exp \frac{\int_0^1 \hat{\alpha}_v(\eta) d\eta}{\lambda - \kappa}, \quad (5)$$

and the dissipation functional is expressed in the form

$$d^g [\hat{\alpha}, \dot{\hat{\alpha}}] = \int_0^1 p_{x0} \exp \left(\frac{\int_0^1 \hat{\alpha}_v(\eta) d\eta}{\lambda - \kappa} \right) \eta \sqrt{\dot{\hat{\alpha}}_v^2 + M^2 \dot{\hat{\alpha}}_s^2} d\eta, \quad (6)$$

where p_{x0} is the initial coordinate of the outer modified cam clay yield surface, c is the parameter determining the shape of the stress-strain curve ($c = 2$ gives a simple hyperbola), and the rest of the definitions are the same as in the PB1 model. The dissipation functional produces a field of elliptical yield surfaces with their centres initially on the p' -axis at p_{x0} as indicated in Figure 2. This point is not necessarily the required initial stress state. A preliminary stress path is needed in order to bring the stress state to the required initial position (indicated by a dot in Figure 2). Figure 2a shows the orientation of the yield surfaces before the sample preparation, and an example of a possible stress path during sample preparation is drawn in a dashed line. Figure 2b shows the yield surfaces after the sample preparation and before the test loading.

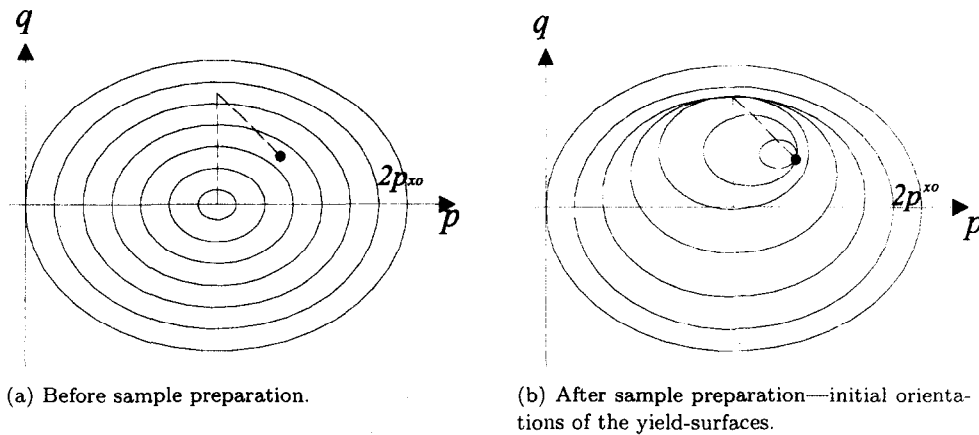


Figure 2. CHMCC1 yield-surfaces.

4.2. Continuous Hyperplastic MCC Model with Aging (CHMCC2)

This model is an extension for the CHMCC1 model to take into account aging effects. In the CHMCC2 model, it is assumed that if, after a loading process, the current stresses are maintained for a sufficient period of time, aging is complete and no further changes in stiffness will occur. Complete aging is simulated in this model by centering the yield surfaces in a linear order on a

line connecting the center of the large-scale yield surface with the required initial stress state. The model is defined by following Gibbs free energy functional

$$\begin{aligned}
 g[p, q, \hat{\alpha}] = & -\kappa p \left(\log \left(\frac{p}{p_0} \right) - 1 \right) - \frac{(q - q_0)^2}{6pG} \\
 & - \left((p - p_0 + p_{x0}) \int_0^1 \hat{\alpha}_v d\eta + (q - q_0) \int_0^1 \hat{\alpha}_s d\eta \right) \\
 & + \int_0^1 \frac{(1 - \eta)^3}{2(a - 1)} \frac{(p/\kappa)\hat{\alpha}_v^2 + 3pG\hat{\alpha}_s^2}{2} d\eta + (\lambda - \kappa)p_{x0} \exp \left(\frac{\int_0^1 \hat{\alpha}_v(\eta) d\eta}{\lambda - \kappa} \right),
 \end{aligned} \quad (7)$$

and the dissipation functional

$$d^g [\hat{\alpha}, \dot{\hat{\alpha}}] = \int_0^1 \left\{ p_{x0} \exp \left(\frac{\int_0^1 \hat{\alpha}_v(\eta) d\eta}{\lambda - \kappa} \right) \eta \sqrt{\dot{\hat{\alpha}}_v^2 + M^2 \dot{\hat{\alpha}}_s^2} - \eta \frac{q_0}{M} \dot{\hat{\alpha}}_s - \eta (p_0 - p_{x0}) \dot{\hat{\alpha}}_v \right\} d\eta. \quad (8)$$

The dissipation functional produces a field of elliptical yield functions with centers initially located on a line connecting the initial stress point with the p_{x0} point (see Figure 3). Note that we assume that all the yield surfaces (except for the outer one) are affected by the change in the stress-state location. Other assumptions could be made with respect to orientation of the yield surfaces, such as that the only yield surfaces that would need to be relocated are those which were translated during a previous loading. In order to improve the understanding of the effect of aging on the yield surfaces, relevant laboratory tests are necessary.

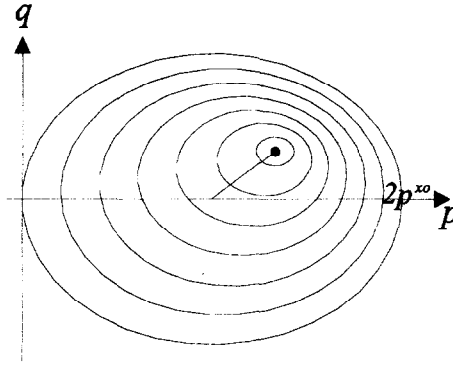


Figure 3. Initial orientation of the CHMCC2 yield-surfaces.

5. EVALUATION OF THE PERFORMANCE OF THE MODELS

5.1. Experimental Data

The four models were evaluated against experimental data obtained on Laval samples of Bothkennar clay by Smith [10]. Figure 4 presents the stress paths adopted for the test program. Nine triaxial tests were performed, following consolidation and swelling along ABCD stress path. Two of the tests were conducted as undrained: one in compression (LCU1) and one in extension (LCU3); and seven as drained (labeled LCDN, where N corresponds to the inclination, in degrees, of the probing stress path to the p' -axis).

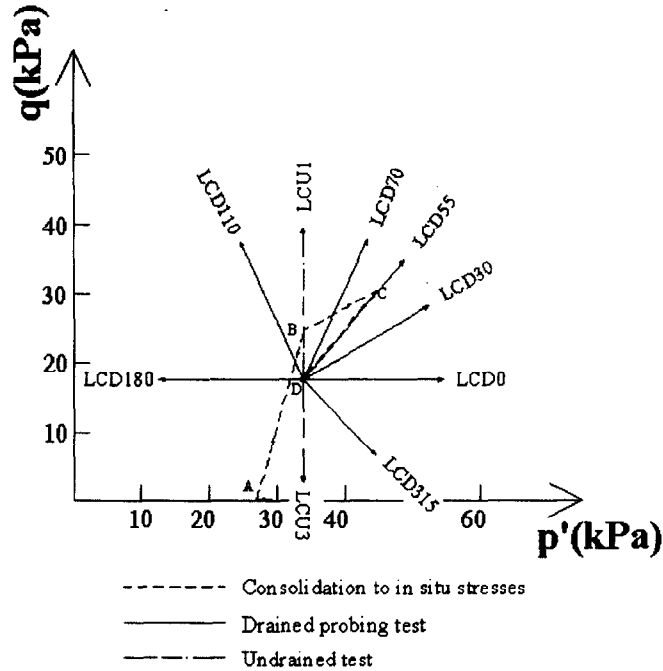


Figure 4. Experimental program for Bothkennar clay (after Smith [10]).

5.2. Evaluation of the Models

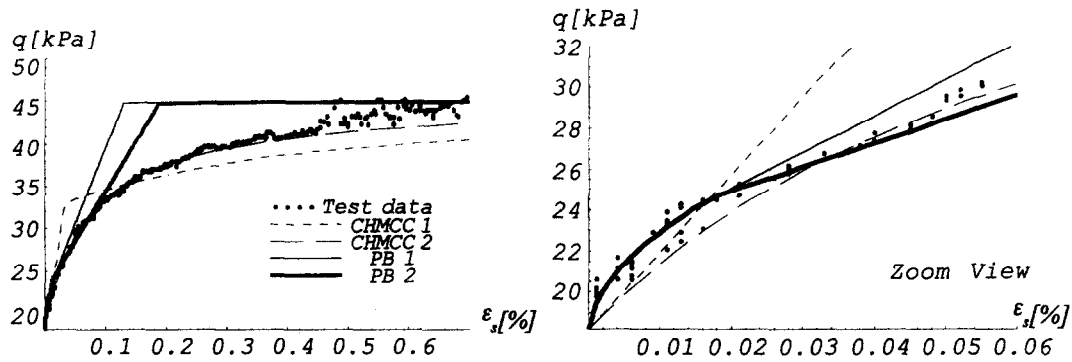
Simulations of only two triaxial tests from the program in Figure 4 are presented: an undrained compression (LCU1) and a drained test with a 70° inclination of the probing stress path to the p' -axis (LCD70).

Figures 5a and 5b present the computer program prediction for the four models for the undrained compression test. It may seem from Figure 5a that the CHMCC2 model is the most accurate one in simulating the overall material behaviour. However, in an enlarged view of this test (Figure 5b); it can be seen that the PB2 model is simulating the small strain stiffness in the best way. The importance of the additional parameter in the PB2 model is well reflected in these figures, where the PB2 stress-strain curve stays closer to the test data than the PB1 stress-strain curve. The advantage of the complete aging consideration in the CHMCC2 model is also confirmed. The kink in the CHMCC1 stress-strain curve is due to the fact that the yield surfaces were initially arranged by previous loading.

Figures 6a and 6b show the theoretical responses and the material behaviour for drained triaxial test LCD70. In Figure 6a, the volumetric stress-strain curves from the CHMCC2, PB1, and PB2 model predictions reasonably agree with the test data. However, the CHMCC1 prediction is less accurate. In Figure 6b, the deviatoric stress-strain curves of the PB models describe the

material behaviour reasonably well. The CHMCC models are somewhat more distant from the test data. Though it seems that the CHMCC2 follows the test data in the small strain region of high stiffness in the best manner, a closer look would have revealed that PB models are more accurate.

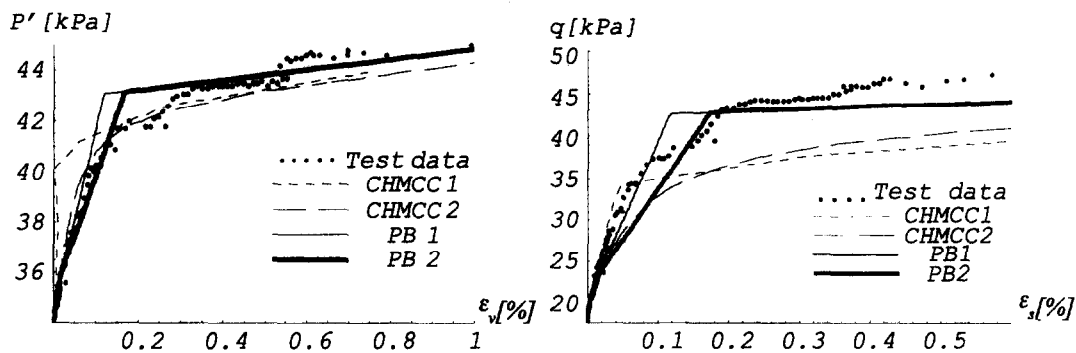
The purpose here has been to demonstrate that alternative models can be rapidly developed and compared within the continuous hyperplasticity framework. It is not intended that any of the models presented here are the best possible for describing lightly overconsolidated clays. Rather they represent some early attempts to achieve the important objective of bringing together small strain stiffness and critical state soil mechanics in a single theoretical framework.



(a) Undrained triaxial LCU1 on Bothkennar clay (deviatoric stress-strain curve).

(b) Enlarged view of Figure 5a.

Figure 5.



(a) Drained triaxial test LCD70 on Bothkennar clay (volumetric stress-strain curve).

(b) Drained triaxial test LCD70 on Bothkennar clay (deviatoric stress-strain curve).

Figure 6.

6. CONCLUSIONS

The ability of the continuous hyperplasticity to reformulate existing kinematic hardening plasticity models and to formulate entirely new models is demonstrated. Only two scalar potential functionals have to be generated in order to define a new constitutive model. These functionals are the input for a new constitutive modelling computer program which makes the process of constitutive modelling almost automatic.

Nonlinearity and stress-path dependency of soil behaviour is considered to be an important issue in geotechnical engineering. It has been demonstrated that a variety of reasonably accurate models of different complexity, which focus on various aspects of these phenomena, can be easily formulated within the continuous hyperplastic framework.

REFERENCES

1. A.M. Puzrin and G.T. Houlsby, A thermodynamical framework for rate-independent dissipative materials with internal functions, *International Journal of Plasticity* **16**, 1017–1039, (2000).
2. A.M. Puzrin and G.T. Houlsby, Fundamentals of kinematic hardening hyperplasticity, *International Journal of Solids and Structures* **38**, 3771–3794, (2001).
3. H. Ziegler, *An Introduction to Thermomechanics*, North-Holland, Amsterdam, (1977); Second Edition, (1983).
4. G.T. Houlsby, A study of plasticity theories and their applicability to soils, Ph.D. Thesis, University of Cambridge (1981).
5. I.F. Collins and G.T. Houlsby, Application of thermomechanical principles to the modelling of geomaterials, *Proc. Royal Society of London, Series A* **453**, 1975–2001, (1997).
6. G.T. Houlsby and A.M. Puzrin, A thermomechanical framework for constitutive models for rate-independent dissipative materials, *International Journal of Plasticity* **16**, 1017–1047, (2000).

7. Z. Mroz and V.A. Norris, Elastoplastic and viscoplastic constitutive models for soils with application to cyclic loads, In *Soil Mechanics—Transient and Cyclic Loads*, (Edited by G.N. Pande and O.C. Zienkiewicz), pp. 173–218, Wiley, (1982).
8. A.M. Puzrin and J.B. Burland, Kinematic hardening plasticity formulation of small strain behaviour of soils, *International Journal of Numerical Analytical Methods in Geomechanics* **24**, 753–781, (2000).
9. A.M. Puzrin, G.T. Houlsby and J.B. Burland, Thermomechanical formulation of a small strain model for overconsolidated clays, *Proceedings of the Royal Society of London, Series A* **457** (2006), 425–440, (2001).
10. P.R. Smith, Properties of high compressibility clays with reference to construction on soft ground, Ph.D. Thesis, University of London, (1992).
11. J.B. Burland, Small is beautiful—The stiffness of soil at small strains, Ninth Laurits Bjerrum Memorial Lecture, *Canadian Geotechnical Journal* **16**, 499–516, (1989).
12. R.J. Jardine, D.M. Potts, A.B. Fourie and J.B. Burland, Studies of the influence of non-linear stress-strain characteristics in soil-structure interaction, *Géotechnique* **36**, 377–396, (1986).
13. R.J. Jardine, Some observations on the kinematic nature of soil stiffness, *Soils and Foundations* **32**, 111–124, (1992).
14. A.M. Puzrin and J.B. Burland, Nonlinear model of small-strain behaviour of soils, *Géotechnique* **48**, 217–233, (1998).
15. R. Butterfield, A natural compression law for soils (an advance on $e - \log p'$), *Géotechnique* **29**, 469–480, (1979).